Division of Engineering
BROWN UNIVERSITY
PROVIDENCE, R. I.

THE DYNAMIC STRESS-STRAIN RELATION OF LEAD AND ITS DEPENDENCE ON GRAIN STRUCTURE

J. M. GONDUSKY and J. DUFFY

Department of the Navy
Office of Naval Research
Contract Nonr-562(20)
Task Order NR-064-424
Technical Report 53

Nonr-562(20)/53

May 1967

Nonr-562(20)/53

THE DYNAMIC STRESS-STRAIN RELATION OF LEAD AND ITS DEPENDENCE ON GRAIN STRUCTURE

by

J. M. Gondusky and J. Duffy

Technical Report No. 53
Division of Engineering
Brown University
Providence, Rhode Island

May 1967

Sponsored by
Department of the Navy
Office of Naval Research
Under Contract Nonr-562(20)
Task Order NR-064-424

THE DYNAMIC STRESS-STRAIN RELATION OF LEAD AND ITS DEPENDENCE ON GRAIN STRUCTURE[1]

by

J. M. Gondusky[2] and J. Duffy[3]

Abstract

Several specimens of commercial and high-purity lead of various grain size and crystallographic orientation were loaded dynamically in compression by means of the split Hopkinson bar. Strain rate was held constant at approximately 1200 sec^{-1} for strains up to about 15%. The dynamic stress-strain curves were found to lie approximately 50% higher than the corresponding static curves.

The compression tests described formed part of a larger project whose purpose was to determine dynamic values of Tabor's constant for lead and its dependence on crystal orientation. For this purpose the results of the compression tests were combined with those of dynamic indentation tests previously performed on the same lead specimens. It was found that dynamic values of Tabor's constant range from 2.4 to 6.0 depending upon grain size and orientation. These values are approximately equal to the corresponding static values. They may be compared to the value of 2.8 obtained by Tabor and other investigators for numerous fine-grained polycrystalline materials, including lead, and for strains up to about 20%.

---

1 The results presented in this paper were obtained in the course of research sponsored by the Office of Naval Research under Contract Nonr-562 (20) with Brown University.

2 Member of Research and Development Technical Staff, Texas Instruments Incorporated, Attleboro, Mass.

3 Professor of Engineering, Brown University.

1. INTRODUCTION

A proportional relationship between the true stress in simple compression, σ, and an average applied pressure, P, required to produce an equivalent strain in a ball indentation test was first proposed by Tabor.[1]* According to this relation

$$C = P/\sigma$$

and for fine-grained polycrystalline materials it was found that C is indeed very nearly constant and approximately equal to 2.8.

In an investigation of the dynamic stress-strain relation of metals, Mok and Duffy[2] compared the values of yield stress as found by indentation using a hard ball to the corresponding values in simple compression. Tabor's constant, C, was found to be just a few percent above the value of 2.8 for both static and dynamic tests on an annealed steel and for two annealed aluminum alloys. However, the tests on lead gave a value of 3.59 which is significantly greater. At the same time, Mok and Duffy reported that only the lead had exhibited "non-axial symmetric yielding" which, in the case of a ball indentation, involved alternate "piling-up" and "sinking-in" of the material about the perimeter of the indentation. When viewed from above, the indentation appeared to be "squarish".

Similar indentation flow patterns have been observed in static tests by other investigators[3,4] for single crystals of aluminum and copper which also have a face centered cubic structure. This led Dudderar and Duffy[5] to the idea that the most likely source of the deformation patterns would be an orientated substructure possibly involving grains of a size comparable to the indentations. To investigate this idea and to see if grain size or

---

* Numbers in brackets refer to references listed at the end of this paper.

orientation influences the value of Tabor's constant, they prepared several surfaces and specimens of lead with careful attention to grain size and crystallographic orientation. They determined the static and dynamic indentation pressure, P, for each surface using a one inch steel ball. Simple static compression tests at strain rates of about 0.001 sec^{-1} also were carried out in a commercial testing machine. From these data, values of the static Tabor's constant, C, were found to range from 2.25 to 5.50.

The present study deals with determination of the dynamic stress-strain relation for specimens of lead of various grain size and crystallographic orientation at a strain rate of about 1200 sec^{-1}. The dynamic Tabor's constant for these specimens is computed using the results of ball indentation tests performed by Dudderar and Duffy.[5]

2. PREPARATION OF SPECIMENS

The specimens used in the dynamic simple compression tests were all machined from large lead billets. A total of 27 such specimens were tested representing nine different grain sizes or orientations as described in the Table. In the undeformed state the specimens were right circular cylinders 0.400" in diameter and 0.400" long. They were machined from material directly beneath undeformed portions of the surface following the indentation tests on these same surfaces. Each specimen was polished chemically and etched on all surfaces to remove all plastically deformed material. Crystallographic orientation was determined by the standard Laue x-ray method.[6] The specimens tested were as follows:

(a) Four specimens from large single crystals of 99.99% lead grown in the laboratory. These were machined so the (001), (012), (111) and (135) planes were parallel to the impact face.

(b) A fine-grained polycrystalline structure obtained from a 99.99% lead billet by straining about 30% and allowing recrystallization. The grain size ranged from 1.5 to 5.0 mm. (maximum dimension).

(c) Four specimens obtained from a commercially cast billet of 99.9% lead (the same metal used by Mok and Duffy). This billet was first cut transversely at the mid-plane to give a columnar grain structure and to reproduce as closely as possible the surface used by Mok and Duffy in their indentation tests. One set of specimens was machined so their geometric axes were normal to the midplane of the billet. These are referred to as the columnar specimens. A second transverse cut near the bottom of the billet provided the "true bottom" (equiaxed) surface and a third cut was taken 18° off this surface. Again, specimens were taken so their geometric axes lay normal to these surfaces. Finally, the long equiaxed surface was obtained by a longitudinal cut near the edge of the billet perpendicular to the columnar face and thus perpendicular to the long grain axes which lay in the preferred growth direction [001]. The "long equiaxed" specimens had axes normal to this face.

3. DYNAMIC COMPRESSION TESTS

The dynamic compression tests were conducted using the Hopkinson pressure bar in the arrangement first devised by Kolsky[7,8]. This split Hopkinson bar technique is reviewed by Davies and Hunter[9] and was further developed by Lindholm[11]. As shown in Figure 1, the cylindrical lead specimen was placed between the two long elastic bars, and the impact produced by a mass striking one end of the bar system.

It was important that strain rate be held as nearly constant as possible throughout each test, and to achieve this the carriage had a fairly large mass (12.6 lbs.) A typical strain-time curve is shown in Figure 2. The carriage travelled on a horizontal rail system at a velocity of about 20 ft./sec. A commercial "Hyge" gun, employing high pressure nitrogen, was used to accelerate the carriage. This arrangement provided a momentum sufficient to insure a substantially constant carriage velocity throughout the loading period of about 100 μ sec.

The method of Karman and Duwez[10] was adopted to terminate the impact rapidly thus serving further to maintain the strain rate as nearly constant as possible. For this purpose, a disk of brittle material was fastened to the carriage (Figure 3). The overall thickness of the disk was 1/2" to prevent bending and premature fracture. However, a deep and sharp groove was machined on one face leaving a thickness of only 0.015" which thus allowed the disk to fracture readily and provided a rapid unloading of the compression pulse upon contact with the anvil.

Since the velocity of the carriage is important, especially in calibration of the system, a means of measurement was included. Immediately before impact, a stiff steel pin fastened to the moving carriage made contact with two stationary thin brittle wires which fractured immediately upon impact. Each contact completed a trigger circuit which allowed a digital counter to record the time interval (Figure 4).

The impact arrangement described provides an elastic stress wave, σ_i, of rapid rise time, and fairly constant amplitude which propagates down the incident pressure bar toward the specimen. A portion, σ_r, of this compressive loading pulse is reflected from the first interface, while part is

transmitted through the specimen. The transmitted wave is in turn partially reflected at the second interface and partially transmitted so that the transmitter bar receives a stress pulse, σ_t. Since the transit time within the specimen is small compared to the duration of the main loading pulse, many internal reflections occur within the specimen during the duration of loading. The stress distribution in the specimen is thus fairly homogeneous and plastic deformation takes place quite uniformly in the lead specimen. The compressive stress wave, σ_t, travels to the free end of the transmitter bar where it is reflected as a tension wave to return to the specimen. Since the interface between transmitter bar and specimen cannot support tension, this stress wave assumes the role of an unloading pulse and separation occurs between the specimen and the transmitter bar.

The Hopkinson bars in the present tests were made of 2024-T4 aluminum, had a 1/2" diameter and were 40" long. The length to diameter ratio was chosen to avoid dispersive effects between the gage stations and the interfaces with the specimen. The bars remained elastic throughout the tests. The impact end of the incident bar was centered in the anvil with a free fitting teflon bushing. The two bars were joined by a sliding teflon collar. Light thread slings supported this collar and also the free end of the transmitter bar. Thus the entire bar system was essentially ballistically suspended and free from all axial restraint. One end of each Hopkinson bar was polished to a fine finish taking great care to preserve the normality of the faces to the axis of the bar. A thin layer of silicone grease was placed between these faces and the specimen to insure uniform contact and freedom for lateral expansion of the specimen. A special depth gauge was also used to set the initial extension, δ_o, of the incident pressure bar (Figure 3).

An accuracy of $\pm$ 0.001" was provided by the gauge and thus afforded a fine control on the amount of total deformation in the specimen.

To monitor the loading pulse type C-5 electric resistance strain gages were bonded to the Hopkinson bars. Two gages were bonded on opposite sides of the incident bar at a distance of 20" from the specimen. Two gages were also bonded on opposite sides of the transmitter bar at a distance of 14" from the specimen. Bending effects were eliminated by making each pair of gages the opposite arms of two D-C bridges. These bridges were completely separated with individual power supplies to eliminate any interaction. A bridge excitation voltage of 6.0 volts was used for the incident gages while 18.0 volts was necessary to insure a sufficiently high output for the gages on the transmitter bar.

The output of each bridge was then amplified and displayed on a dual beam Tektronix Type 555 oscilloscope (Figure 4). Type 1A1 plug-in signal amplifiers were chosen for their wide band pass (21 m.c.) and high gain (5mv./cm.). The incident bridge output became the input for channel #1 of the upper beam amplifier and for channel #1 of the lower beam amplifier. The transmitter bridge output became the input for channel #2 of the lower beam amplifier. Thus with only channel #1 operative in the upper beam amplifier and with the lower beam amplifier operating in a chop mode, three traces were displayed on the screen of the oscilloscope. A single sweep of the upper beam was triggered by the carriage as it cut a light beam directed toward a photocell immediately before the point of contact with the incident bar. A delay was introduced into the trigger of the lower beam time-base.

Through the use of the apparatus as described above, continuous strain-time histories were obtained of the incident pulse, ε_i, the reflected

pulse, ε_r, and the transmitted pulse, ε_t. Recording was accomplished by a polaroid camera mounted on the oscilloscope. A typical photograph is shown in Figure 5.

4. ANALYSIS OF MEASUREMENTS

The experiment provides the strain-time history of the incident, the reflected and the transmitted pulses. Since the two bars remain elastic throughout the test, the stress and particle velocity can be determined at each interface as functions of time. From the elementary theory of elastic wave propagation in slender bars we know that

$$u = C_o \int_o^t \varepsilon \, dt$$

where u is the displacement at the time t, C_o the elastic wave velocity, and ε the strain. The displacement u_1 of the face of the incident bar is the result of both the incident strain pulse ε_i travelling in the positive x direction and of the reflected strain pulse ε_r travelling in the negative x direction. Thus

$$u_1 = C_o \int_o^t \varepsilon_i \, dt - C_o \int_o^t \varepsilon_r \, dt$$

or

$$u_1 = C_o \int_o^t (\varepsilon_i - \varepsilon_r) \, dt$$

The displacement u_2 of the face of the transmitter bar is obtained from the transmitted strain pulse ε_t travelling in the positive x direction, so that

$$u_2 = C_o \int_o^t \varepsilon_t \, dt$$

The nominal strain in the specimen ε_s is then

$$\varepsilon_s = \frac{(u_1 - u_2)}{l_o} = \frac{C_o}{l_o} \int_o^t (\varepsilon_i - \varepsilon_r - \varepsilon_t) \, dt$$

where l_o is the initial length of the specimen. The expression may be simplified if we take the stress across the short specimen as constant, since then $\varepsilon_r = \varepsilon_t - \varepsilon_i$ and ε_s becomes

$$\varepsilon_s = - \frac{2 C_o}{l_o} \int_o^t \varepsilon_r \, dt \qquad (1)$$

The applied loads P_1 and P_2 on each face of the specimen are

$$P_1 = A E (\varepsilon_i + \varepsilon_r)$$

and

$$P_2 = A E \varepsilon_t$$

where E is the modulus of elasticity of the pressure bars and A their cross-sectional area. Thus, the average stress in the specimen σ_s is

$$\sigma_s = \frac{(P_1 + P_2)}{2A_s} = \frac{1}{2} E(A/A_s) (\varepsilon_i + \varepsilon_r + \varepsilon_t)$$

where A_s is the cross-sectional area of the specimen. This expression may be simplified by taking the stress constant within the specimen, so that

$$\sigma_s = E\,(A/A_s)\,\varepsilon_t \qquad (2)$$

Hence, when the gage calibration is known, stress and strain in the specimen may be found at any time from the value of $\varepsilon_t(t)$ and the area contained beneath the curve $\varepsilon_r(t)$. In the present tests the values of stress and strain were calculated at the end of each 10 μ sec. interval along the pulse length. This provided a series of points which determined the strain-time curve and the stress-strain curve.

In the derivation of equations (1) and (2) the stress is taken as constant along the length of the specimen. This is sufficiently accurate if the specimen is short compared to the wave length. In the present tests no barreling or flared ends were observed on the deformed specimens indicating not only a lack of lateral frictional restraint, but a state of fairly uniform compressive strain. In addition, the experiment affords a more positive check on the validity of the relation $\varepsilon_i = \varepsilon_r + \varepsilon_t$. The pulses ε_r and ε_t were fed as inputs to a differential amplifier and the sum displayed as the lower beam on the oscilloscope. This sum was compared to the display of ε_i on the upper beam. All differences between the two were within the accuracy with which the photograph could be measured.

There is another check of results which usually can be made. The total strain in the specimen can be found after impact by a measurement of the final deformed length. This total strain should equal the total strain computed on the basis of the oscillograph records. Unfortunately this check could not be made for the present tests because the strain gages on the

incident bar were too near the impact end (14 inches). As a result the reflected pulse was incomplete because of a second reflection which occurred at the impact end.

It should also be pointed out that equations (1) and (2) give the engineering stress and strain in the specimen. For comparison with indentation tests, all data have been plotted as true stress and true strain by use of the equations

$$\sigma_T = (1 - \varepsilon) \tag{3}$$

$$\varepsilon_T = \ln (1 - \varepsilon) \tag{4}$$

where σ and ε are stress and strain in the specimen at the time t as given by equations (1) and (2). Equations (3) and (4) are valid for the compression tests if the material behaves incompressibly in the plastic range of deformation.

Davies and Hunter[9] have investigated extensively the split Hopkinson bar and have given a stress correction factor for radial and longitudinal inertia effects in the specimen. According to these authors the stress σ_s in the specimen is given in terms of the stress σ_m at the surface in contact with the transmitter bar through the relation

$$\sigma_s = \sigma_m + \rho_s \left[\frac{1}{6} l_o^2 - \frac{1}{8} \gamma_s^2 d^2 \right] \ddot{\varepsilon}_s$$

where ρ_s and γ are the density and Poisson's ratio of the specimen material, l_o and d are the length and diameter of the specimen, and $\ddot{\varepsilon}_s$ is the second time derivative of the strain. In their tests, specimens of dimensions $l = \sqrt{3/4}\, \gamma_s d$ were employed to make the inertia correction term vanish. Another way to make it vanish is to hold the strain rate $\dot{\varepsilon}_s$

constant. In the present tests, much attention was paid to the design of the loading apparatus in order to achieve a constant strain rate. As a result the strain-time plot was very closely linear in each test as may be seen in Figure 2, a typical strain-time history. Whereas the strain-rate remained constant for any given test its value could not be set with any precision. However, all tests were in the range 1100 sec.$^{-1}$ to 1300 sec.$^{-1}$.

With the Hopkinson bar it is possible to make an accurate dynamic calibration of the instrumentation if the velocity of the impact carriage is known. Since the bar remains elastic we may write for the particle velocity

$$\frac{du}{dt} = \frac{du}{dx} \cdot \frac{dx}{dt} = \varepsilon \cdot C_o$$

and, since upon impact the particle velocity assumes the velocity of the carriage V, we have

$$\left(\frac{du}{dt}\right)_{max} = V$$

so that

$$\varepsilon_{max} = V/C_o$$

Hence, when V and C_o are known one can find the maximum strain.

5. EXPERIMENTAL DATA & DISCUSSION OF RESULTS

The results of the dynamic tests in simple compression are presented in Figures 6 through 14. Each figure represents several tests of one particular grain size or crystallographic orientation, and individual specimens are distinguished by a symbol. The values plotted represent stress and strain at the end of 10 μ sec. intervals of loading, so that a line connecting points

represented by one particular symbol would constitute the complete stress-strain curve for that specimen. Other specimens are assigned different symbols so individual stress-strain curves can be drawn for all tests. However, in each figure only one stress-strain curve is actually drawn. It represents an average of all specimens with one orientation and grain size.

Figures 6 through 14 also show the corresponding dynamic indentation test data obtained by Dudderar and Duffy.[5] Tabor's constant has been calculated in each case to provide the best correlation with the simple compression data. The Table presents the static value of Tabor's constant as reported in Reference 5 for each orientation and grain size tested and the dynamic value of this constant determined through the present investigation.

Large differences in the deformation patterns of the ball indentations were noted in Reference 5. Both round and squarish indentations were observed and correlated with the crystallographic orientation of the indented surface. Similar variations in the deformation patterns were also noted in the dynamic compression tests. Figure 15 shows full size photographs of typical compression specimens for each of the nine orientations and grain sizes investigated. A study of these specimens reveals the similarities with the deformation patterns around the ball indentations, and a comparison of deformation patterns in the two types of tests follows.

The four specimens taken from the commercially cast lead billet with the columnar grain structure have fairly high Tabor's constants. The columnar face contained grains approximately 2 to 4 mm in diameter by 60 mm long with the long axis of the columnar grain lying in the preferred growth or [001] direction. The compression specimens in which impact occurred on the columnar face exhibited an oblong squarish shape following impact (specimen 5, Fig. 15). For the same face, impact with a spherical ball gave

a squarish indentation (Figure 8, Reference 2, and Figure 1, Reference 5). In both cases the deformation pattern is probably due to the four-fold symmetry of the (111) slip plane about the direction of impact. It should be remembered that preferred growth is in the [001] direction. By contrast, the long equiaxed, the true bottom and the 18° off bottom specimens exhibited an essentially circular although extremely irregular deformed shape in compression (specimens 6,7 and 8, Fig. 15). This is consistent with the circular shape obtained in the ball indentation tests. The long equiaxed specimens taken perpendicular to the columnar surface had a more uniformly orientated grain structure. The [001] directional misalignment was approximately 2° to 3°. In the true bottom surface the [001] axes were also essentially parallel but were found to be within $\pm 5^{\circ}$ of the normal to the indentation surface. To suppress further the dependence on the [001] orientation, tests were made on a surface 18° off bottom. The dependence of Tabor's constant on the [001] orientation is shown clearly by the results. The lowest value of Tabor's constant occurs for the 18° off bottom surface; it is higher on the true bottom, and highest on the long equiaxed specimens. It should also be pointed out that the cross-section of the long equiaxed, the true bottom, and the 18° off bottom specimens includes several grains. Thus the four-fold symmetry of the (111) slip planes will not produce an elongated specimen for these three equiaxed samples (irregular round indentations) as it did for the columnar specimen (square indentations) as shown in Figure 15.

As expected, the single crystal specimens show a highly non-isotropic flow pattern in the compression tests. The (001), (012), and (135) surfaces, which exhibited squarish indentation patterns in the ball tests, produced an oval cross-section in compression (specimens 1, 2 and 4, Fig. 15). These

three specimens also exhibited varying degrees of shear strain distributed uniformly along their length. In other words the specimens appeared tilted in the direction of the smallest diameter in the oval cross-section. By contrast, indentations on the principal slip plane (111) exhibited round indentations with no hilling. Compression specimens with this orientation remained right circular cylinders after impact (specimen 3, Fig. 15).

For the polycrystalline surface, ball indentations were fairly round (though slightly irregular due to a grain size of 1.5 to 5.0 mm. maximum dimension). In simple compression, the deformed specimens were found to be quite round with a uniform cylindrical deformation pattern (specimen 9, Fig. 15). In general, these specimens exhibited no directional preferrence on deforming.

6. CONCLUSIONS

The experiments described formed part of a larger project whose purpose was to determine values of Tabor's indentation constant for specimens of lead of various grain size and crystallographic orientation under both static and dynamic conditions. To establish Tabor's constant for any material, two series of tests are needed: the first to determine the pressure under a ball indenting the specimen, and the other to find the yield stress in simple compression at a corresponding strain.

The present tests were intended to fulfill the latter purpose. Dynamic stress-strain curves were found for a number of lead specimens in simple compression. Results indicate that, in general, the dynamic ($\dot{\varepsilon}$ = 1200 sec.$^{-1}$) stress is approximately 50% higher than the corresponding static ($\dot{\varepsilon}$ <0.001 sec.$^{-1}$) stress for specimens of lead with different grain sizes and crystallographic orientation. Figure 16 presents the stress-strain curve for

each of four single crystal specimens and for the polycrystalline specimen. Tabor's constant ranges from a low of 2.4 when the indented surface is the principal slip plane (111) itself, to a high of 6.0 for an indentation surface (012) at an angle of about 41° with the principal slip plane. Figure 17 presents the stress-strain curves obtained for the various commercial specimens of lead. The curves form a fairly narrow spectrum since all four commercial samples were essentially polycrystalline. Tabor's constant in this case, ranges only from 4.2 to 4.7. It is evident from the above that the commonly accepted value of 2.8 for Tabor's constant presupposes a fine-grained polycrystalline micro-structure. For single crystals Tabor's constant ranges from 2.4 to 6.0 depending upon the crystal orientation.

ACKNOWLEDGMENT

The authors would like to express their thanks to Dr. T. D. Dudderar and to Mr. R. H. Hawley for their assistance in planning and conducting the experimental work, to Mr. P. Rush for his help in the construction of the test apparatus and the conduction of the experiments, to Mr. R. Pagliarini for his work in the preparation of the specimens and to Miss Piela for typing the manuscript.

TABLE

Values of Tabor's Indentation Constant for Lead

SPECIMEN	IMPACT SURFACE	Tabor's Constant	
		Static	Dynamic
Laboratory cast single Crystal of 99.99% lead.	(111)	2.3	2.4
	(001)	3.75	4.8
	(135)	4.35	5.9
	(012)	5.5	6.0
Recrystallized billet of 99.99% lead (relatively fine grain structure).	any	2.95	4.2
Commercially cast polycrystalline billet of 99.9% lead (columnar grain structure).	orientated 18° to the bottom	3.05	4.2
	true bottom	3.4	4.6
	long equiaxed (i.e. parallel to the geometric axis of the billet)	4.35	4.7
	columnar face at midplane of billet	3.9	4.75

BIBLIOGRAPHY

1. D. Tabor, The Hardness of Metals, Oxford University Press, (1951).

2. C.H. Mok and J. Duffy, "The Dynamic Stress-Strain Relation of Metals as Determined From Impact Tests with a Hard Ball", Int. J. Mech. Sci., 7, 335, (1964).

3. H. O'Neill, "Hardness Tests on Crystals of Aluminum," J. Inst. Metals, 30, 299, (1923).

4. H. Bückle, "Progress in Micro-Indentation Hardness Testing," Met. Rev., 4, 49, (1959).

5. T.D. Dudderar and J. Duffy, "An Investigation of Hilling and The Indentation Pressure-Stress Relations For Ball Tests of Lead", Technical Report No. 52, December, 1966, Contract Nonr 562 (20), Brown University, Providence Rhode Island.

6. B.D. Cullity, "Elements of X-Ray Diffraction," Addison-Wesley Publishing Co., (1956).

7. B. Hopkinson, "A Method of Measuring The Pressure Produced in The Detonation Of High Explosives Or By the Impact of Bullets," Royal Soc. of London, Phil. Trans., A213, 437, (1914).

8. H. Kolsky, "An Investigation of the Mechanical Properties of Materials at Very High Rates of Loading," Proc. Royal Soc. London, B62, 676, (1949).

9. E.D.H. Davies and S.C. Hunter, "The Dynamic Compression Testing of Solids By The Method of the Split Hopkinson Pressure Bar", J. Mech. Phys. Solids, II, 155, (1963).

10. T. von Karman and P.E. Duwez, "The Propagation of Plastic Deformation in Solids," J. Appl. Phys., 21, 987, (1950).

11. U.S. Lindholm, "Some Experiments with the Split Hopkinson Pressure Bar," J. Mech. Phys. Solids, 12, 317, (1964).

12. F.E. Hauser, "Techniques For Measuring Stress-Strain Relations at High Strain Rates," Experimental Mechanics, 6, #8, 395, (1966).

13. R.M. Davies, "A Critical Study of the Hopkinson Pressure Bar," Royal Soc. London-Phil. Trans., A 240, 375, (1948).

14. P.E. Duwez and D.S. Clark, "An Experimental Study of the Propagation of Plastic Deformation Under Conditions of Longitudinal Impact," Proc. A.S.T.M., 47, 502, (1947).

15. E.H. Lee and H. Wolf, "Plastic-Wave Propagation Effects in High-Speed Testing," J. Appl. Mech., 73, 379, (1951).

16. E.T. Habib, "A Method of Making High-Speed Compression Tests on Small Copper Cylinders," J. Appl. Mech., 70, 248, (1948).

17. S.R. Bodner and H. Kolsky, "Stress Wave Propagation in Lead," Nonr Report 562 (14)/6, January 1958, Division of Engineering, Brown University, Providence, Rhode Island.

18. J.N. Greenwood, "The Refining and Physical Properties of Lead," Met. Rev., 6, 23, 279, (1961).

FIGURE CAPTIONS

Figure 1 The split Hopkinson bar used in the present tests.

Figure 2 Strain time history in a typical dynamic simple compression test. Single crystal with impact on (111) face.

Figure 3 Loading arrangement; showing carriage, fracture disk and incident bar.

Figure 4 Instrumentation to measure strains and impact velocity.

Figure 5 Oscillograph record of incident, reflected, and transmitted pulses for a single crystal of lead. Run No. 126; impact occurs on the (111) face.

Figure 6 Dynamic stress and strain for a single crystal of lead in simple compression. Impact occurs on the (111) face. C = 2.4

Figure 7 Dynamic stress and strain for a single crystal of lead in simple compression. Impact occurs on the (001) face. C = 4.8

Figure 8 Dynamic stress and strain for a single crystal of lead in simple compression. Impact occurs on the (135) face. C = 5.9

Figure 9 Dynamic stress and strain for a single crystal of lead in simple compression. Impact occurs on the (012) face. C = 6.0

Figure 10 Dynamic stress and strain for fine-grained polycrystalline lead in simple compression. C = 4.2

Figure 11 Dynamic stress and strain for commercially cast lead in simple compression. Impact occurs on a plane orientated 18° to the true bottom surface of the billet. C = 4.2

Figure 12 Dynamic stress and strain for commercially cast lead in simple compression. Impact occurs on the true bottom surface of the billet. C = 4.6

Figure 13 Dynamic stress and strain for commercially cast lead in simple compression. Impact occurs on the columnar face at midplane of the billet. C = 4.75

Figure 14 Dynamic stress and strain for commercially cast lead in simple compression. Impact occurs on a long equiaxed surface (a plane parallel to the geometric axis of the billet.) C = 4.7

Figure 15 Deformed shapes of lead compression specimens.

Figure 16 The influence of crystal orientation on the dynamic stress-strain relation of single crystals of lead in simple compression.

Figure 17 The anisotropy of a commercially cast lead billet as exhibited by the dynamic stress-strain relation in simple compression. The billet had a columnar grain structure and measured 6 in. in diameter and was 10 in. long.

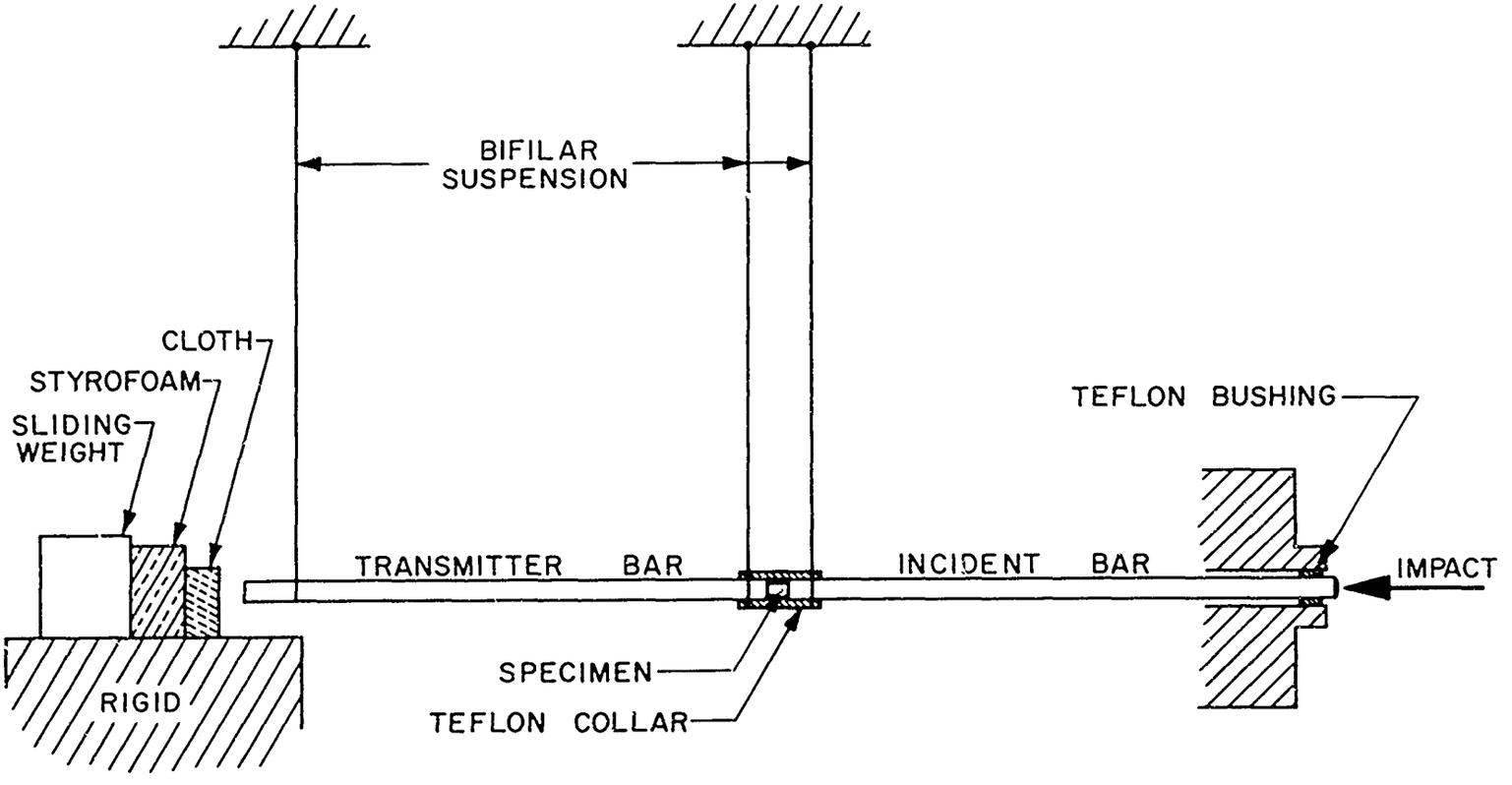
BIFILAR
SUSPENSION
CLOTH
STYROFOAM
SLIDING
WEIGHT
TEFLON BUSHING
TRANSMITTER BAR
INCIDENT BAR
IMPACT
SPECIMEN
TEFLON COLLAR
RIGID

FIGURE 1

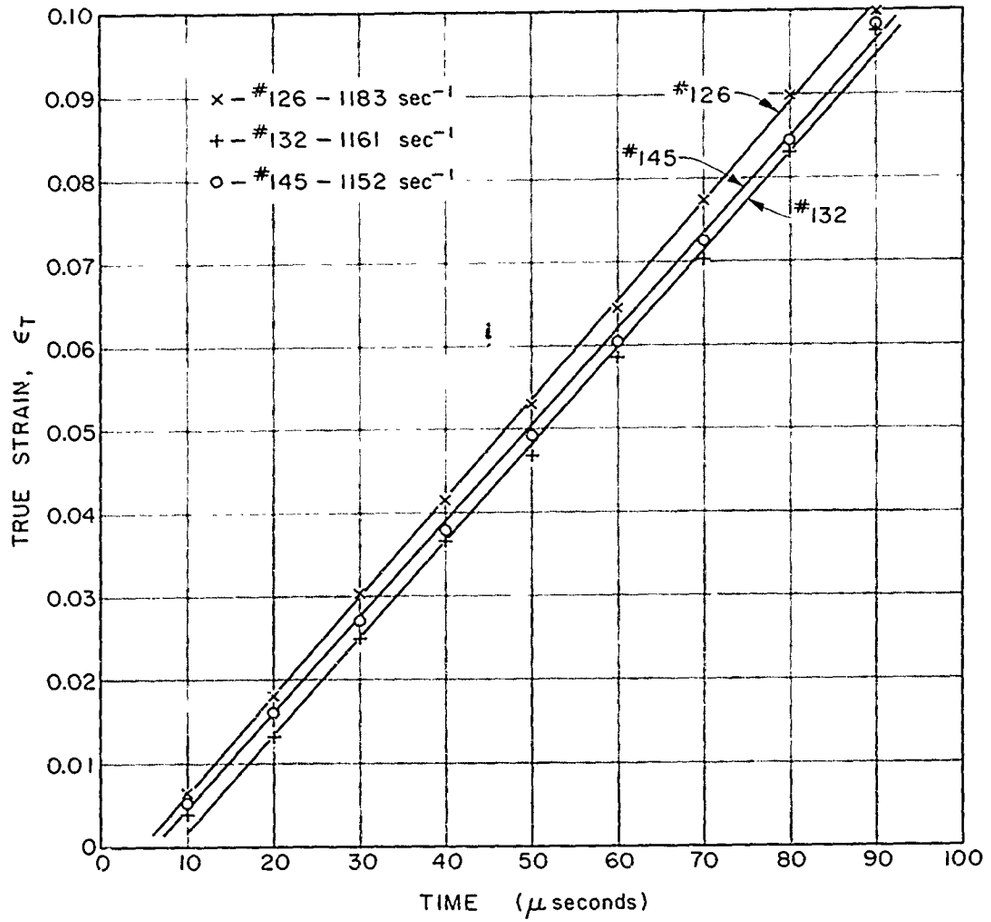
0.10
0.09
0.08
0.07
0.06
0.05
0.04
0.03
0.02
0.01
0
TRUE STRAIN, ϵ_T
× – #126 – 1183 sec^{-1}
+ – #132 – 1161 sec^{-1}
o – #145 – 1152 sec^{-1}
#126
#145
#132
0
10
20
30
40
50
60
70
80
90
100
TIME (μ seconds)

FIGURE 2

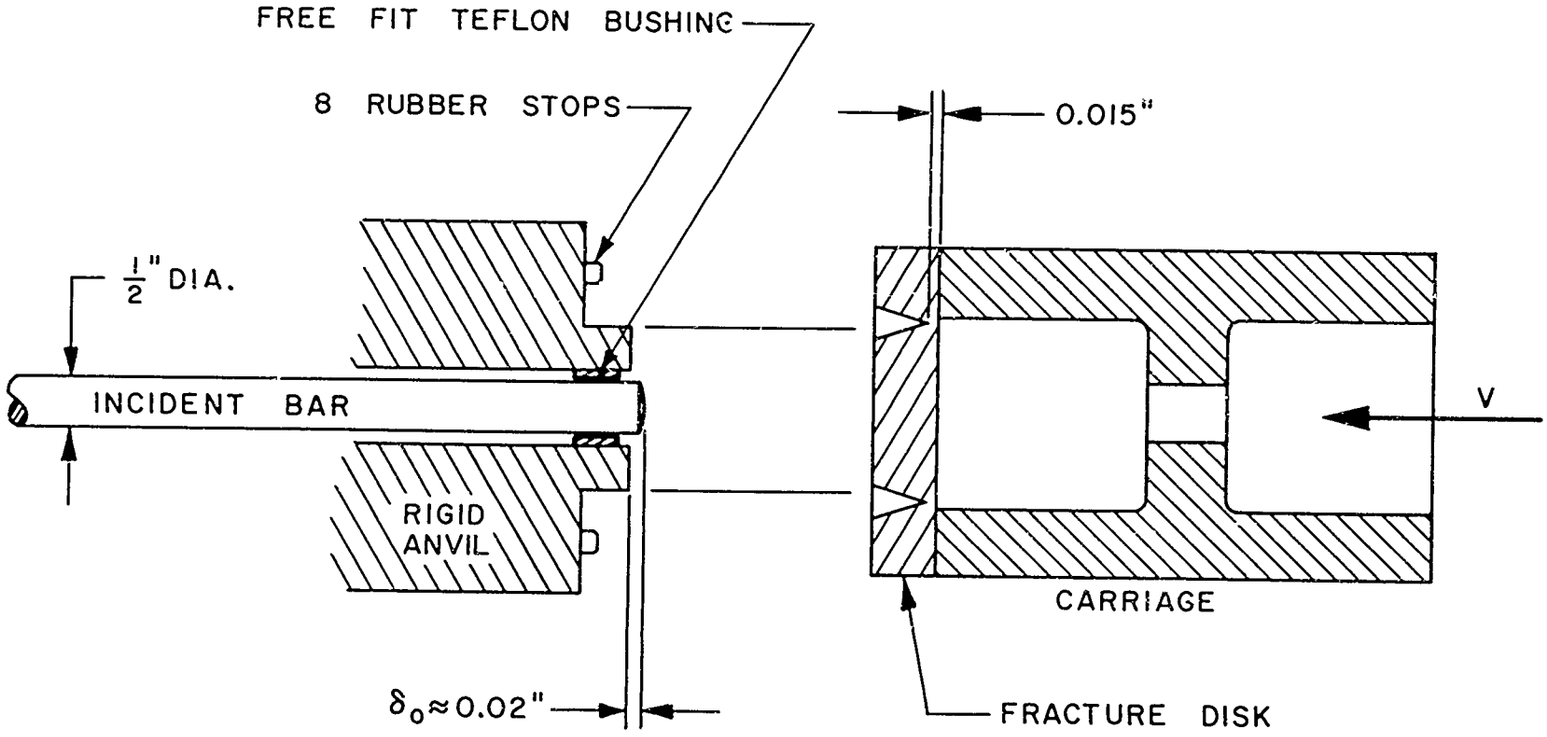
FREE FIT TEFLON BUSHING
8 RUBBER STOPS
0.015"
½" DIA.
INCIDENT BAR
V
RIGID ANVIL
CARRIAGE
$\delta_0 \approx 0.02$"
FRACTURE DISK

FIGURE 3

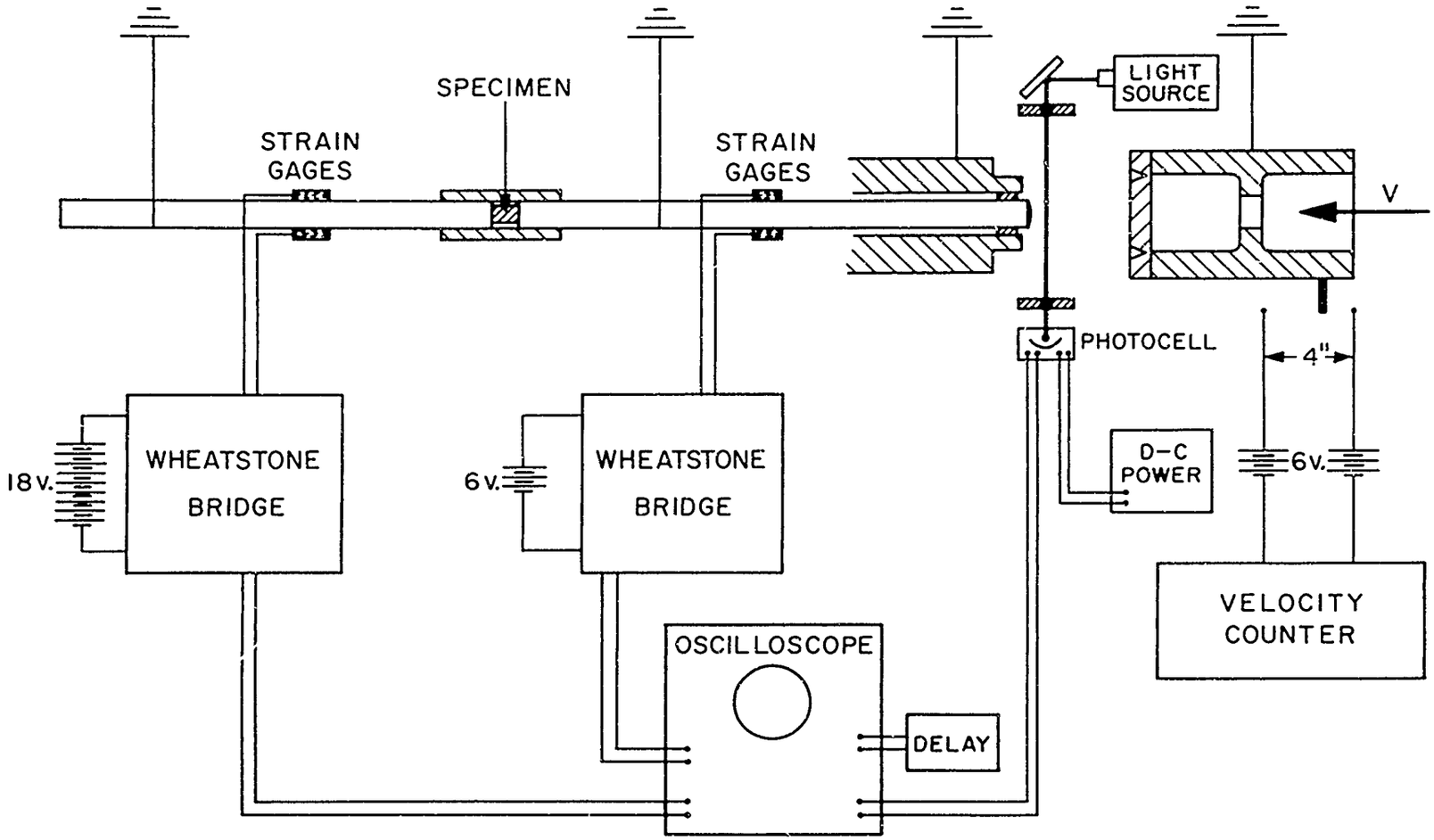
SPECIMEN
STRAIN GAGES
STRAIN GAGES
LIGHT SOURCE
V
PHOTOCELL
4"
18v.
WHEATSTONE BRIDGE
6v.
WHEATSTONE BRIDGE
D-C POWER
6v.
OSCILLOSCOPE
DELAY
VELOCITY COUNTER

FIGURE 4

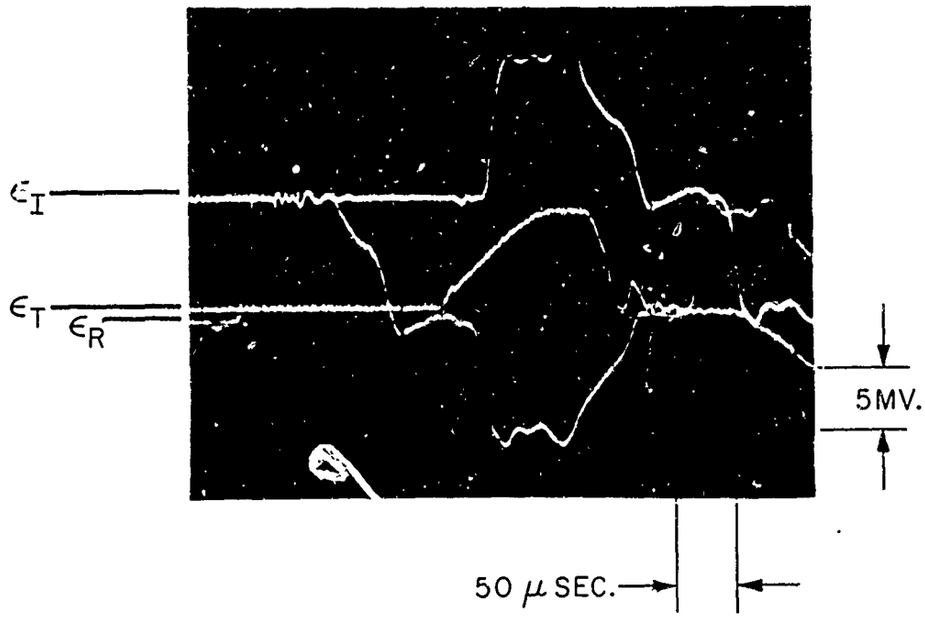

FIGURE 5

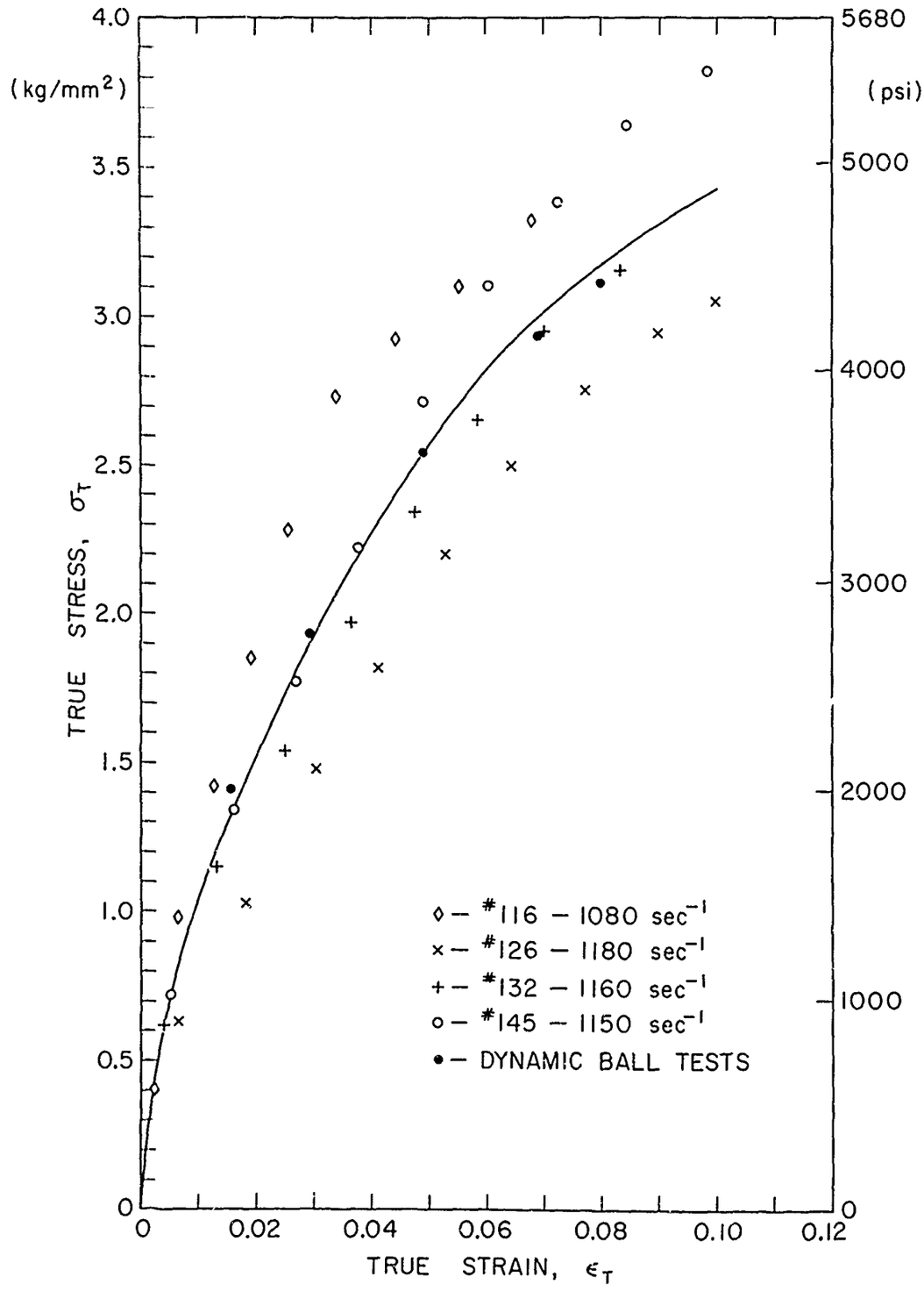
4.0
3.5
3.0
2.5
2.0
1.5
1.0
0.5
0
(kg/mm²)
TRUE STRESS, σT
5680
5000
4000
3000
2000
1000
0
(psi)
0
0.02
0.04
0.06
0.08
0.10
0.12
TRUE STRAIN, εT
◊ — #116 — 1080 sec⁻¹
× — #126 — 1180 sec⁻¹
+ — #132 — 1160 sec⁻¹
○ — #145 — 1150 sec⁻¹
● — DYNAMIC BALL TESTS

FIGURE 6

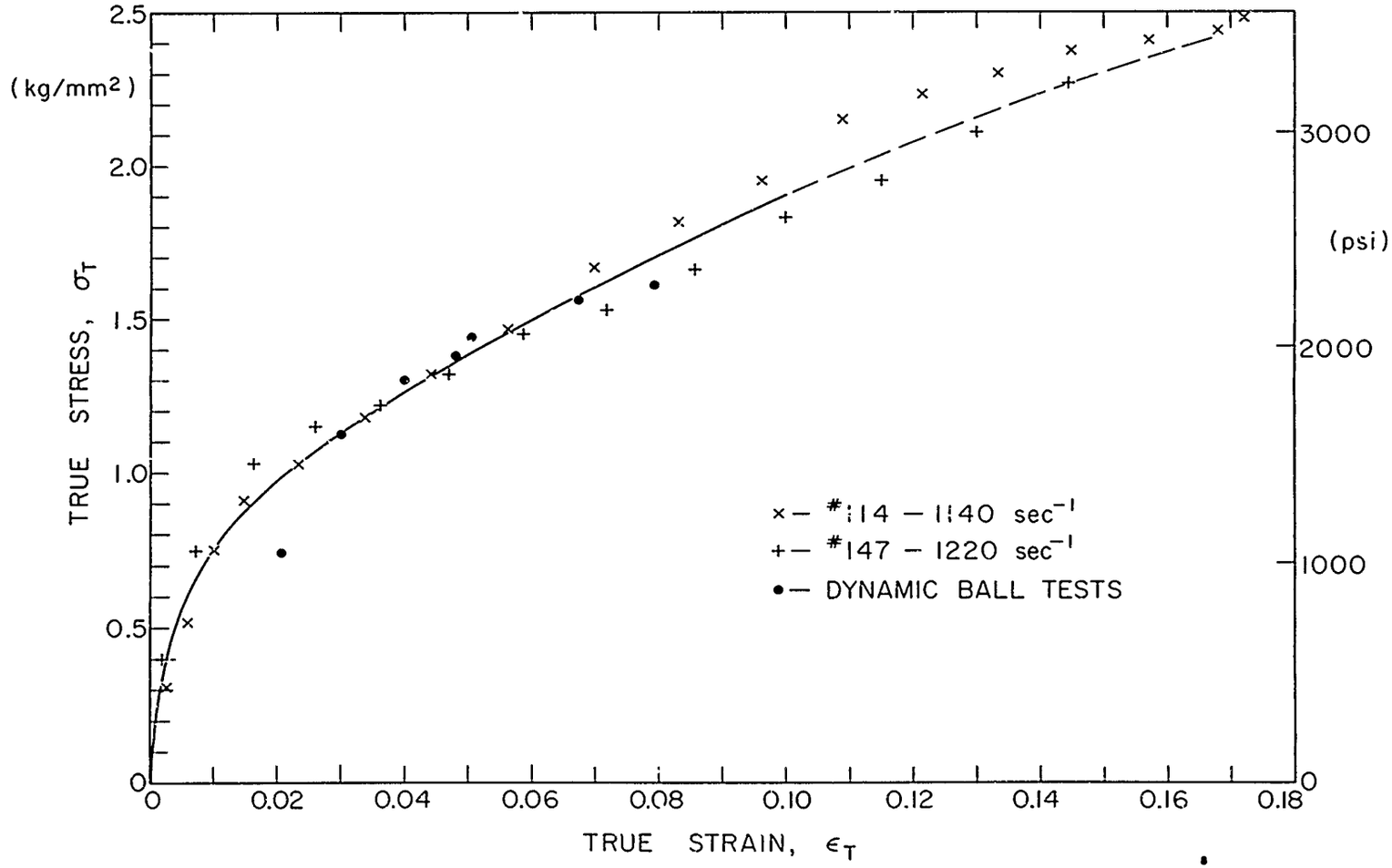
2.5
(kg/mm²)
2.0
1.5
1.0
0.5
0
TRUE STRESS, σ_T
3000
(psi)
2000
1000
0
0
0.02
0.04
0.06
0.08
0.10
0.12
0.14
0.16
0.18
TRUE STRAIN, ϵ_T
× — #114 — 1140 sec⁻¹
+ — #147 — 1220 sec⁻¹
• — DYNAMIC BALL TESTS

FIGURE 7

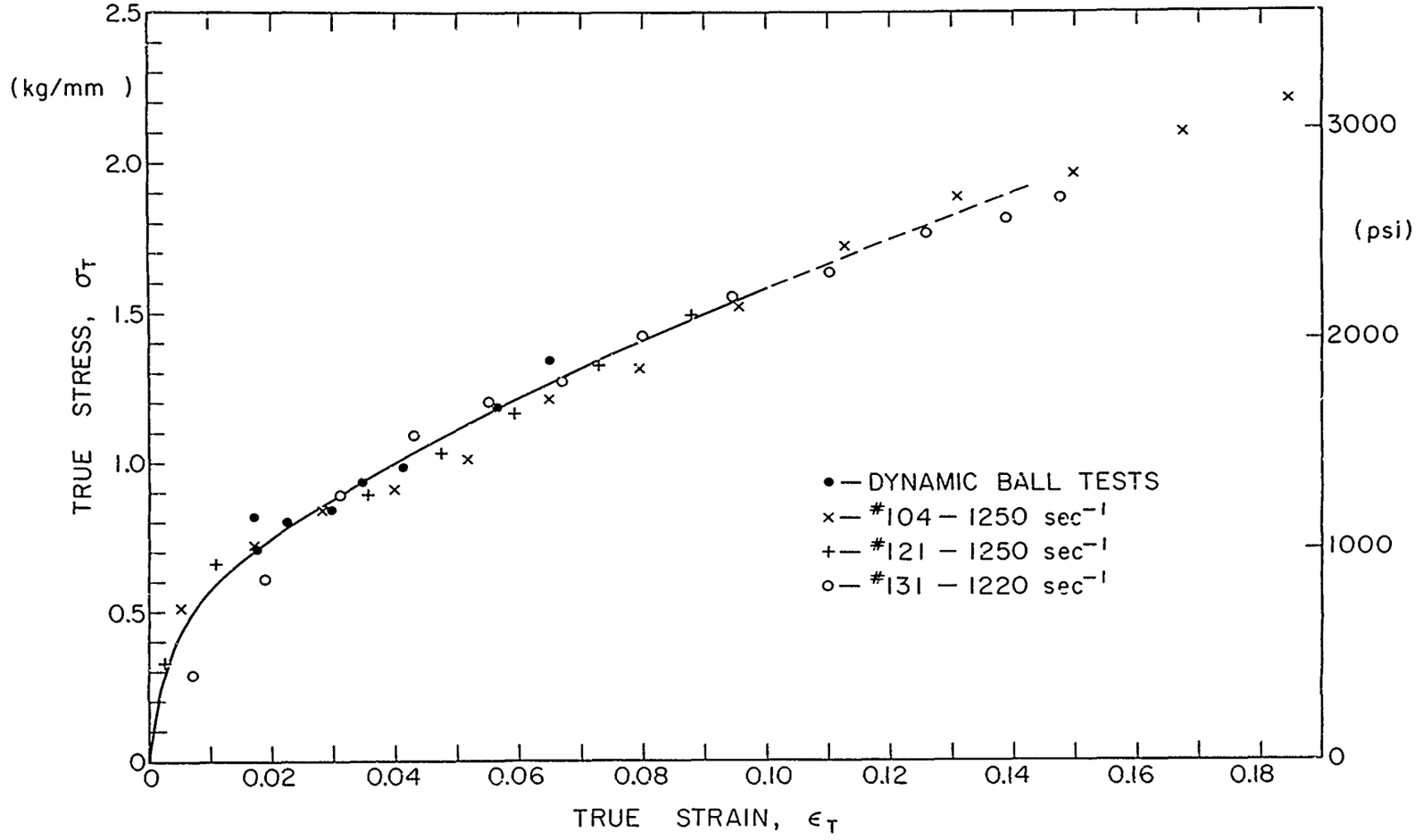
2.5
(kg/mm)
2.0
1.5
1.0
0.5
0
TRUE STRESS, σ_T
3000
(psi)
2000
1000
0
0
0.02
0.04
0.06
0.08
0.10
0.12
0.14
0.16
0.18
TRUE STRAIN, ϵ_T
• — DYNAMIC BALL TESTS
× — #104 — 1250 sec^{-1}
+ — #121 — 1250 sec^{-1}
○ — #131 — 1220 sec^{-1}

FIGURE 8

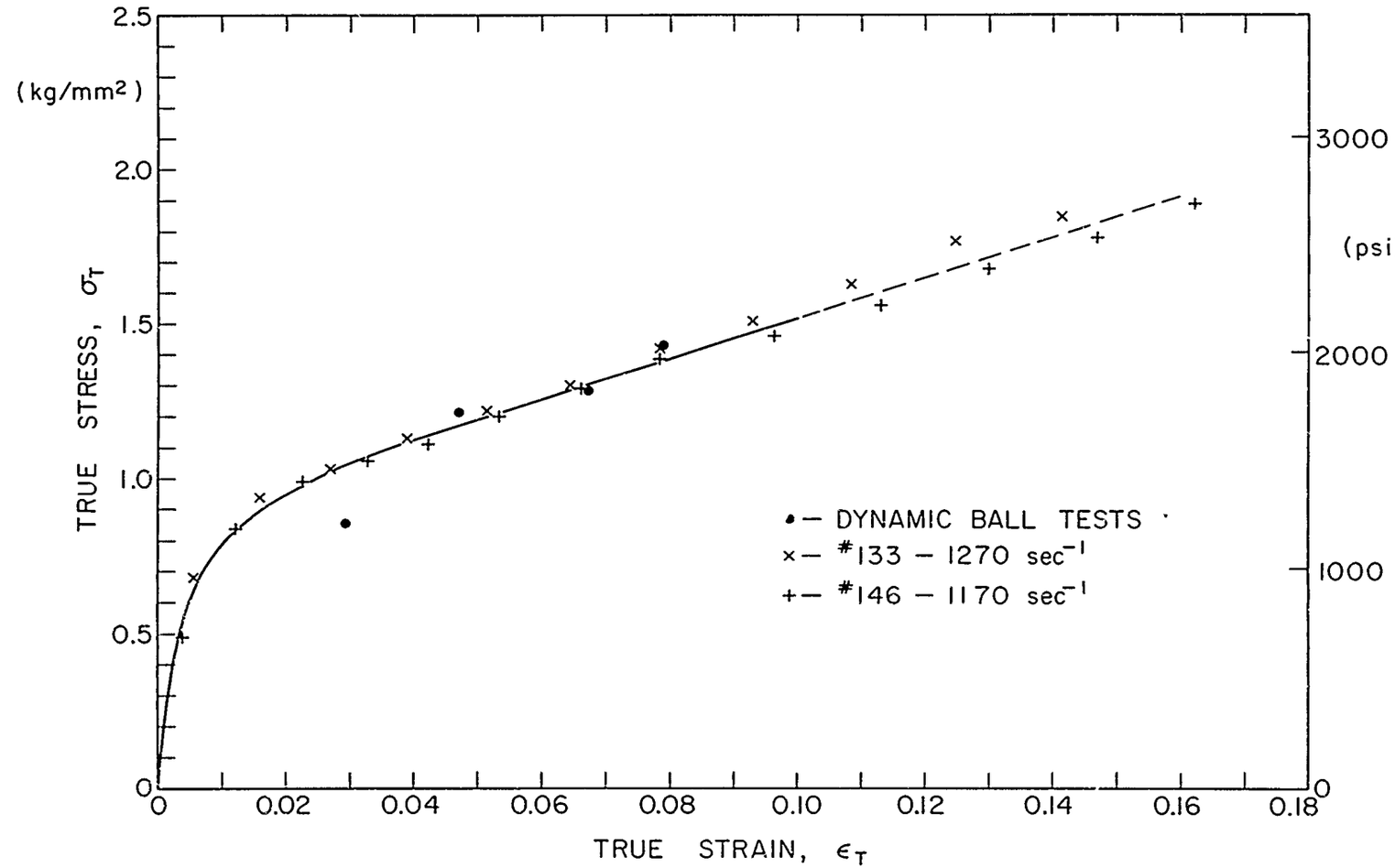
2.5
(kg/mm²)
2.0
1.5
1.0
0.5
0
TRUE STRESS, σ_T
3000
(psi)
2000
1000
0
0
0.02
0.04
0.06
0.08
0.10
0.12
0.14
0.16
0.18
TRUE STRAIN, ϵ_T
• — DYNAMIC BALL TESTS
× — #133 — 1270 sec⁻¹
+ — #146 — 1170 sec⁻¹

FIGURE 9

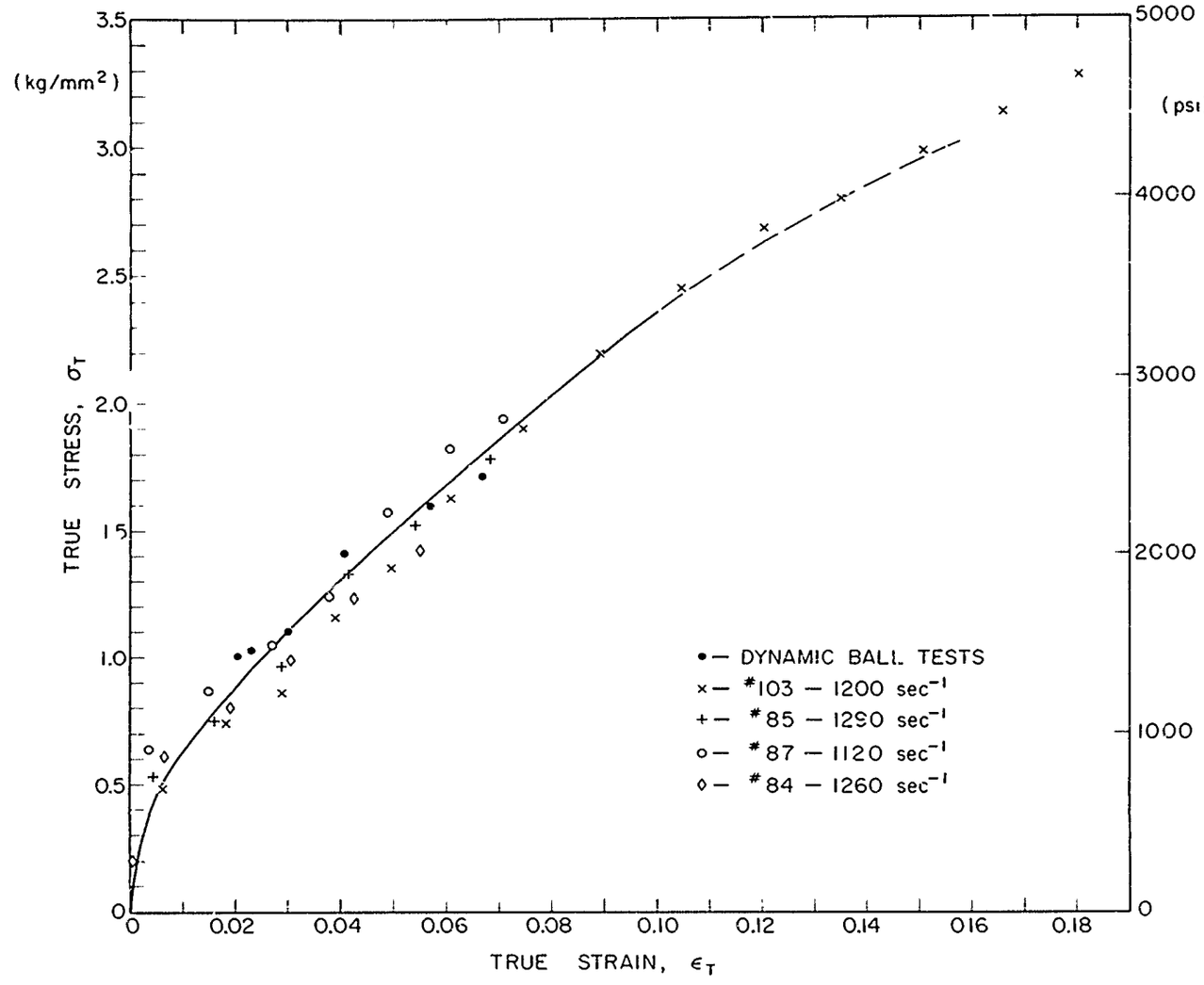
3.5
(kg/mm²)
3.0
2.5
2.0
1.5
1.0
0.5
0
TRUE STRESS, σT
5000
(psi)
4000
3000
2000
1000
0
0
0.02
0.04
0.06
0.08
0.10
0.12
0.14
0.16
0.18
TRUE STRAIN, εT
• — DYNAMIC BALL TESTS
× — #103 — 1200 sec⁻¹
+ — #85 — 1290 sec⁻¹
○ — #87 — 1120 sec⁻¹
◇ — #84 — 1260 sec⁻¹

FIGURE 1C

FIGURE 10

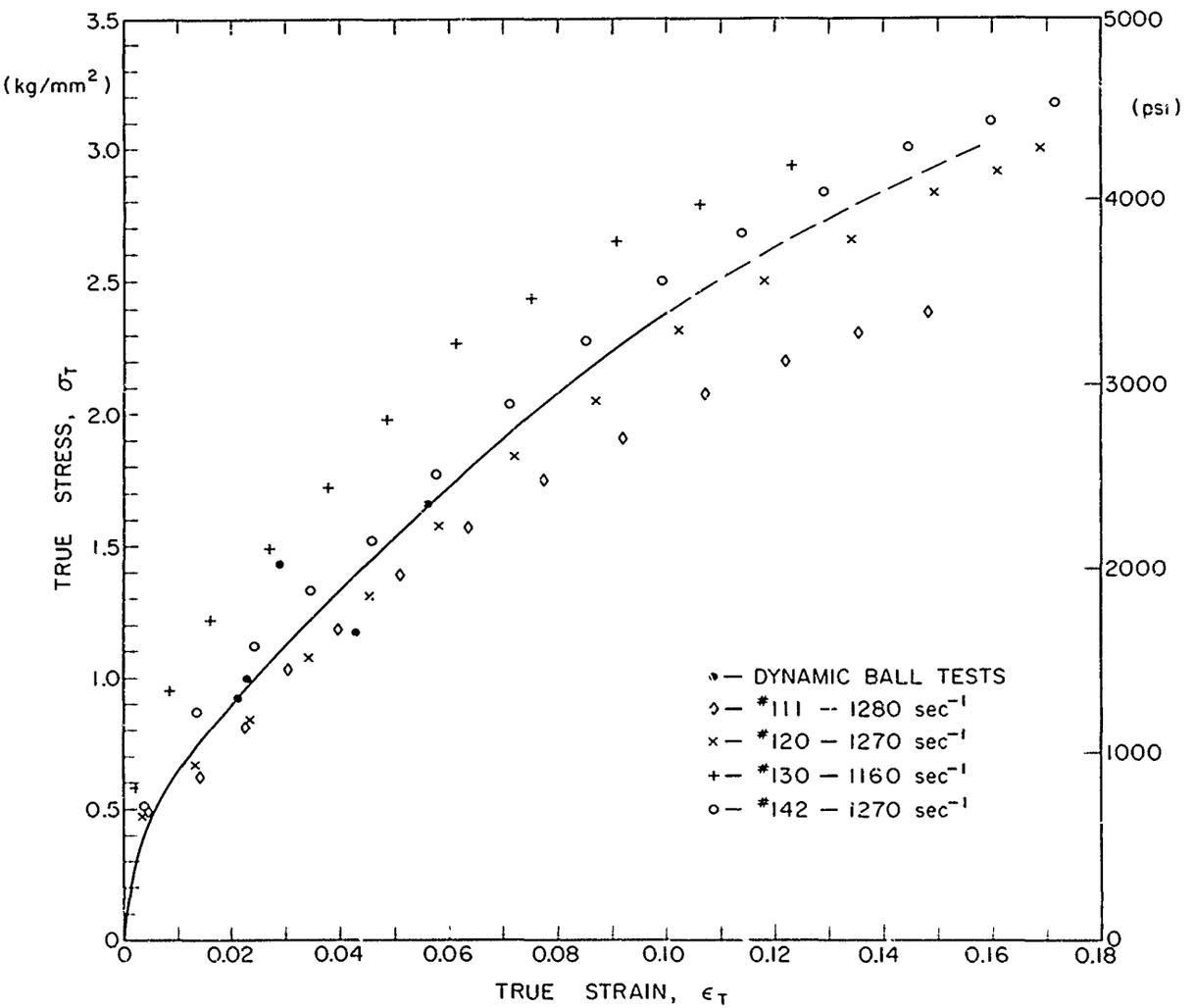

FIGURE 11

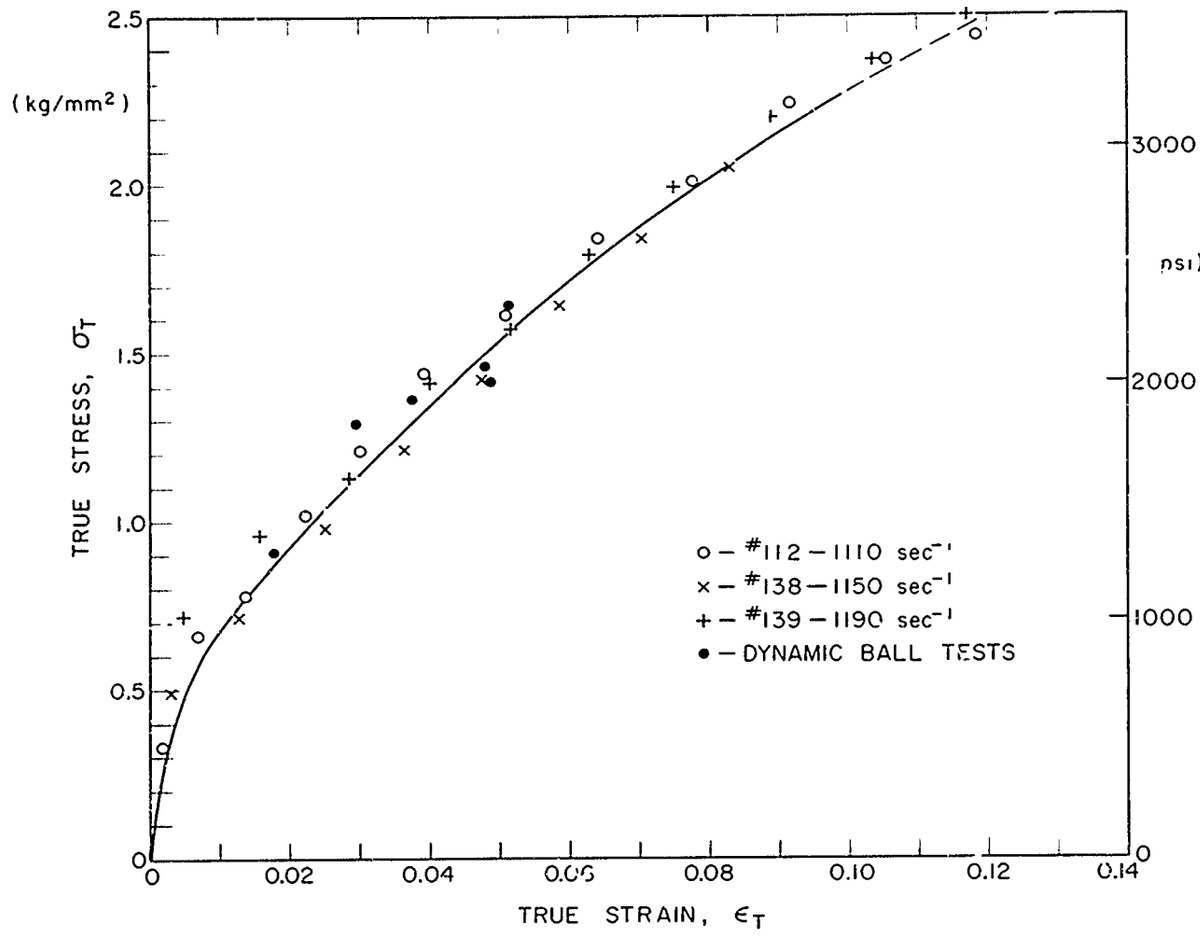
2.5
2.0
1.5
1.0
0.5
0
(kg/mm²)
TRUE STRESS, σT
3000
2000
1000
0
psi)
0
0.02
0.04
0.06
0.08
0.10
0.12
0.14
TRUE STRAIN, εT
o – #112 – 1110 sec⁻¹
× – #138 – 1150 sec⁻¹
+ – #139 – 1190 sec⁻¹
• – DYNAMIC BALL TESTS

FIGURE 12

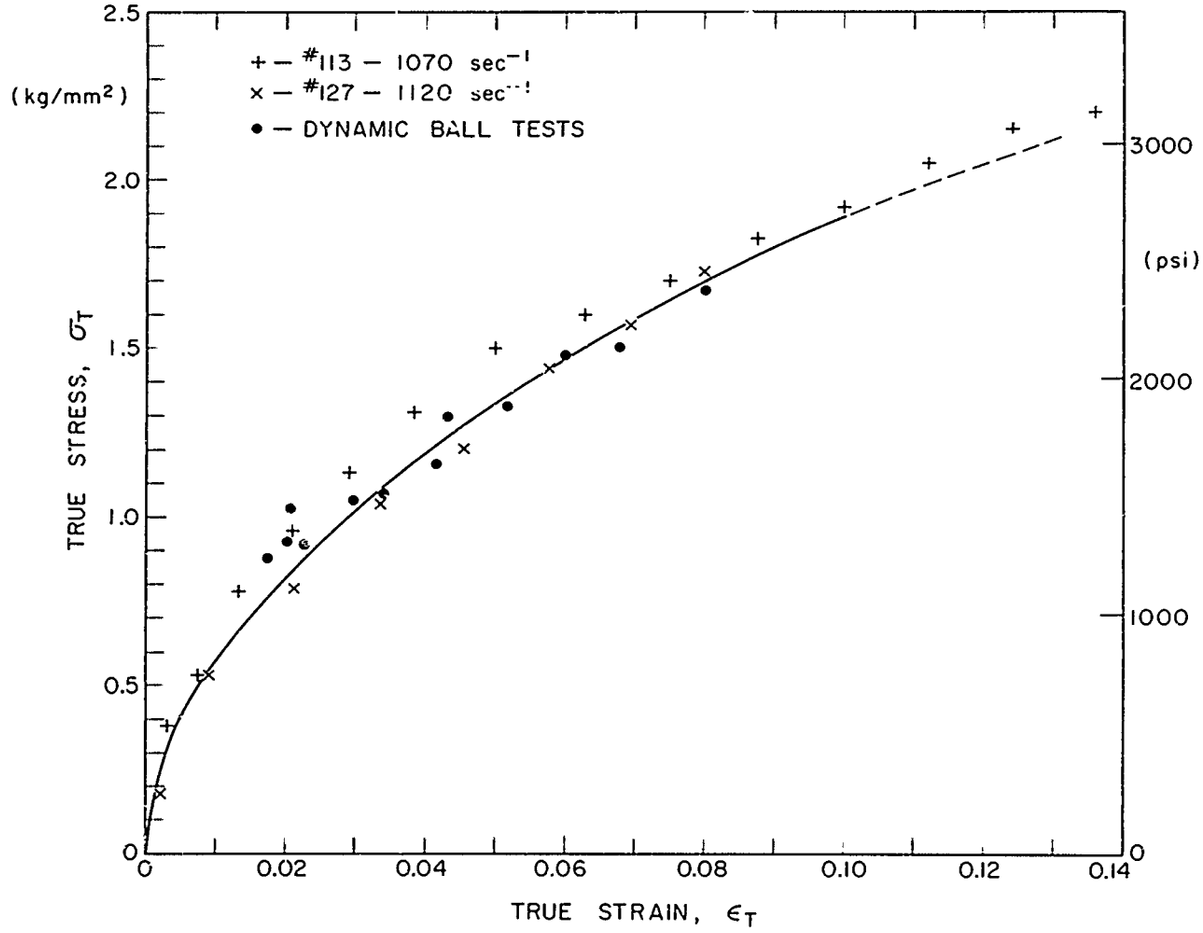
+ — #113 — 1070 sec⁻¹
× — #127 — 1120 sec⁻¹
• — DYNAMIC BALL TESTS
(kg/mm²)
TRUE STRESS, σ_T
(psi)
TRUE STRAIN, ϵ_T
2.5
2.0
1.5
1.0
0.5
0
3000
2000
1000
0
0.02
0.04
0.06
0.08
0.10
0.12
0.14

FIGURE 13

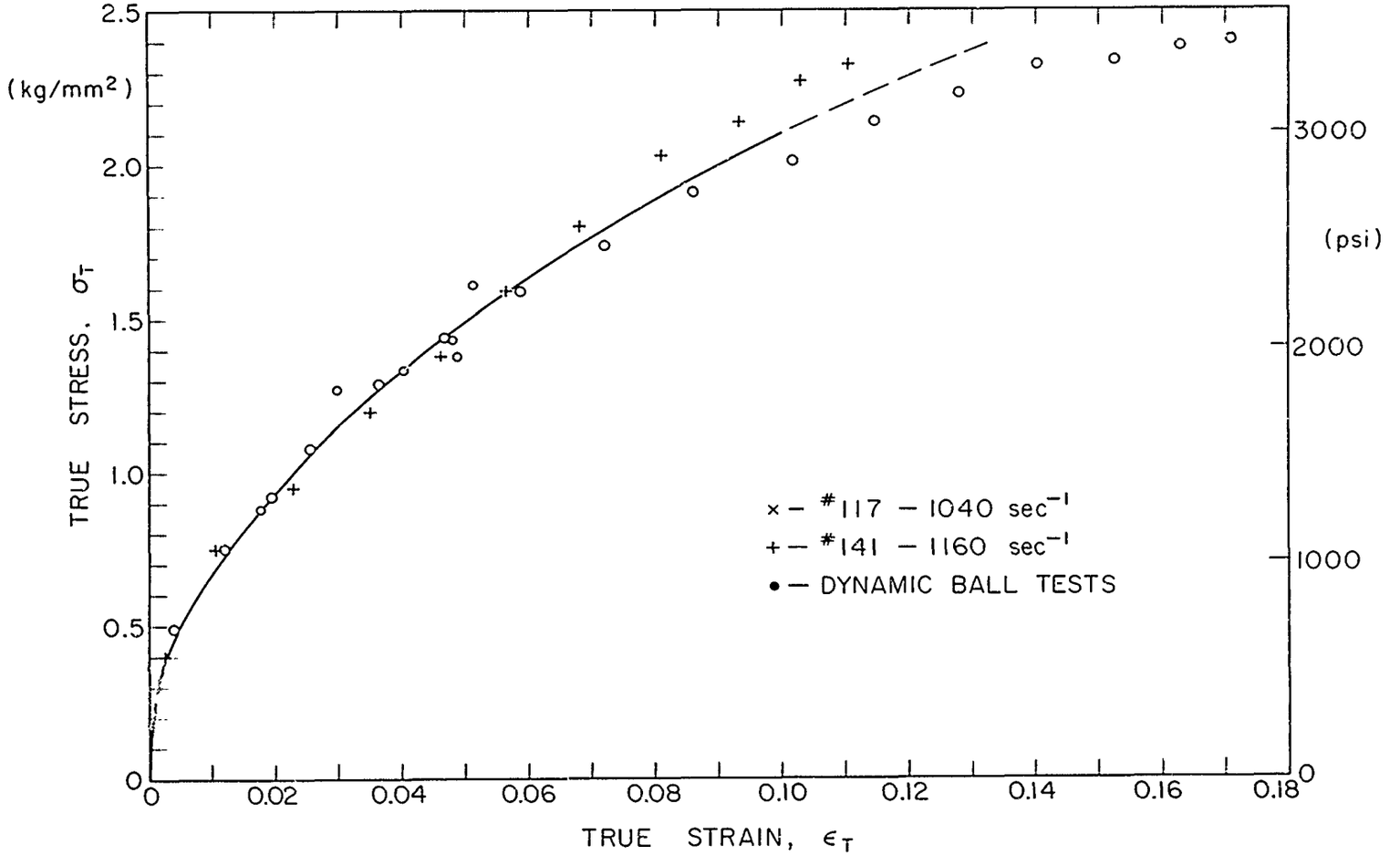
2.5
(kg/mm²)
2.0
1.5
1.0
0.5
0
TRUE STRESS. σ_T
3000
(psi)
2000
1000
0
0
0.02
0.04
0.06
0.08
0.10
0.12
0.14
0.16
0.18
TRUE STRAIN, ϵ_T
× — #117 — 1040 sec⁻¹
+ — #141 — 1160 sec⁻¹
• — DYNAMIC BALL TESTS

FIGURE 14

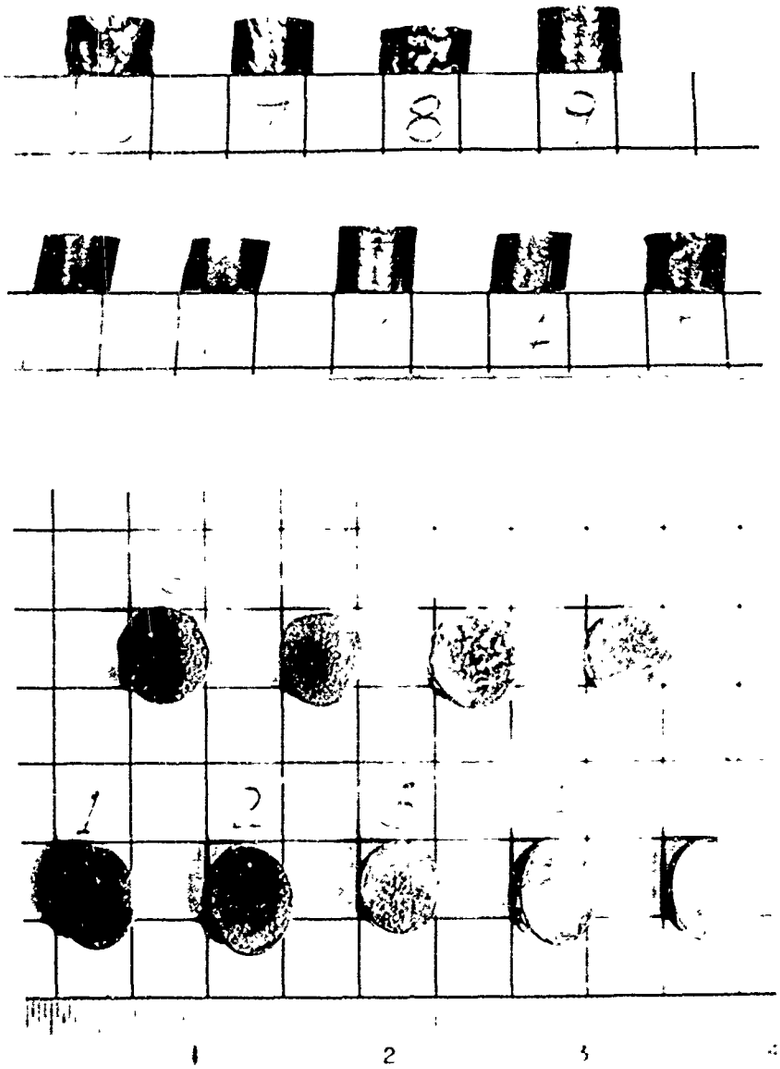

1. (001)
2. (012)
3. (111)
4. (135)
5. COLUMNAR
6. TRUE BOTTOM
7. LONG EQUIAXED
8. 18° OFF BOTTOM
9. FINE GRAINED POLYCRYSTALLINE

FIGURE 15

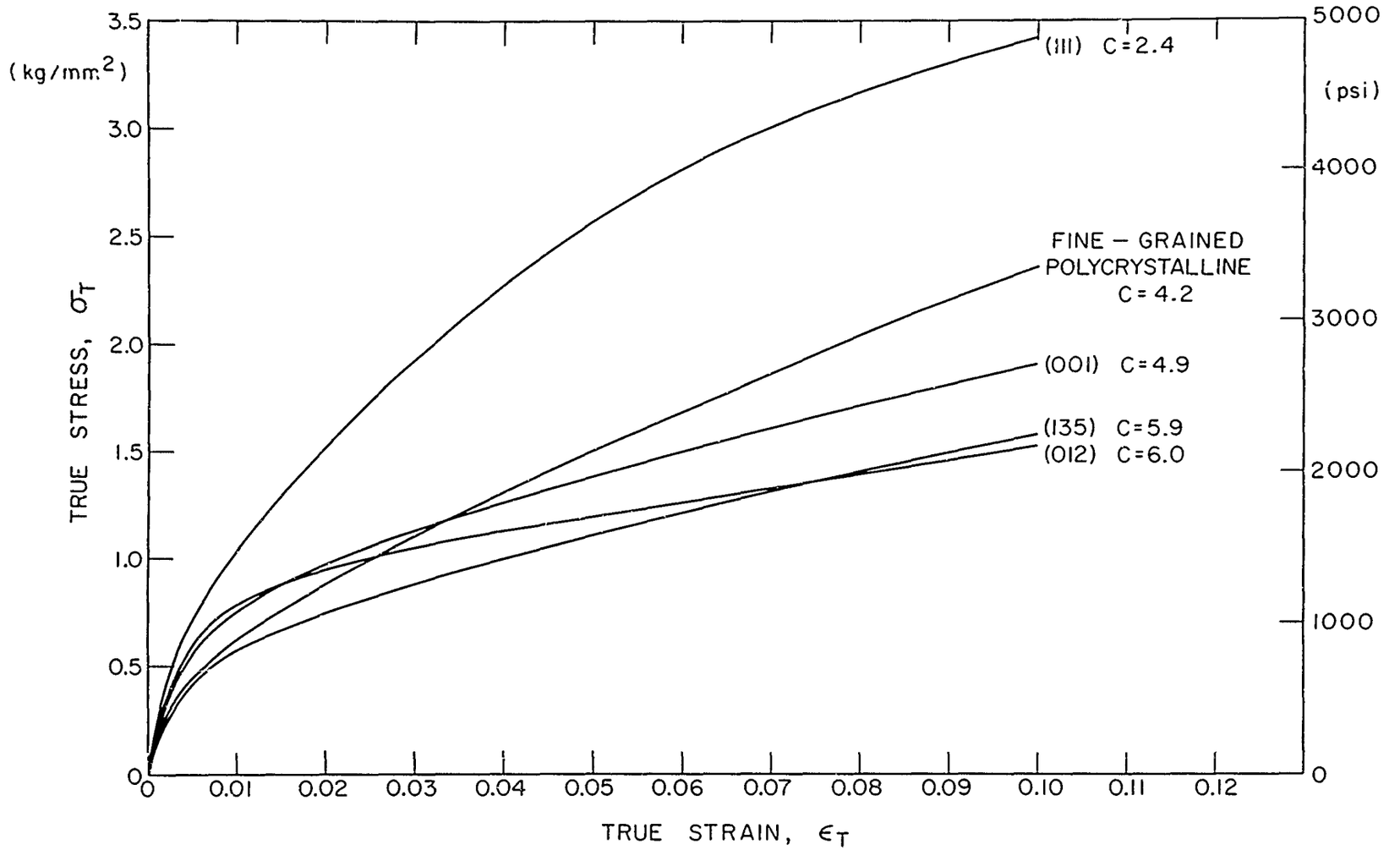
3.5
(kg/mm²)
3.0
2.5
2.0
1.5
1.0
0.5
0
TRUE STRESS, σ_T
5000
(psi)
4000
3000
2000
1000
0
(111) C=2.4
FINE – GRAINED
POLYCRYSTALLINE
C=4.2
(001) C=4.9
(135) C=5.9
(012) C=6.0
0
0.01
0.02
0.03
0.04
0.05
0.06
0.07
0.08
0.09
0.10
0.11
0.12
TRUE STRAIN, ϵ_T

FIGURE 16

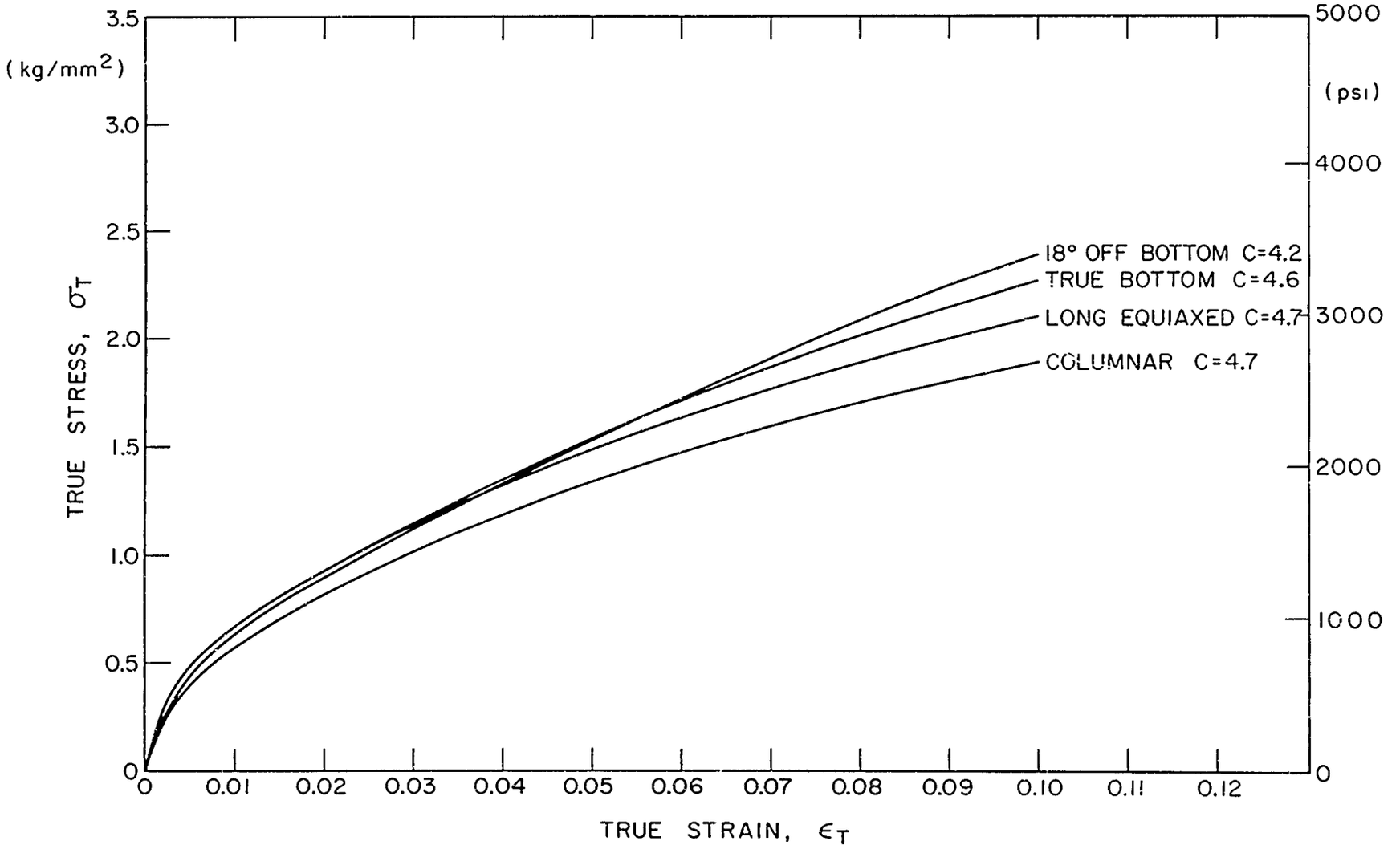
3.5
(kg/mm²)
3.0
2.5
2.0
1.5
1.0
0.5
0
TRUE STRESS, σT
5000
(psi)
4000
3000
2000
1000
0
18° OFF BOTTOM C=4.2
TRUE BOTTOM C=4.6
LONG EQUIAXED C=4.7
COLUMNAR C=4.7
0
0.01
0.02
0.03
0.04
0.05
0.06
0.07
0.08
0.09
0.10
0.11
0.12
TRUE STRAIN, εT

FIGURE 17

Security Classification

DOCUMENT CONTROL DATA - R&D

(Security classification of title, body of abstract and indexing annotation must be entered when the overall report is classified)

1 ORIGINATING ACTIVITY (Corporate author) Brown University, Engineering Division Providence, Rhode Island	2a REPORT SECURITY CLASSIFICATION Unclassified 2b GROUP

3 REPORT TITLE

The Dynamic Stress-Strain Relation of Lead and Its Dependence on Grain Structure

4 DESCRIPTIVE NOTES (Type of report and inclusive dates)

Technical Report

5 AUTHOR(S) (Last name, first name, initial)

Gondusky, J. M.
Duffy, J.

6 REPORT DATE	7a TOTAL NO OF PAGES	7b NO OF REFS
May 1967	38	18

8a CONTRACT OR GRANT NO.	9a ORIGINATOR'S REPORT NUMBER(S)
Nonr - 562 (20) b PROJECT NO c TASK NR #064-424 d.	Nonr - 562 (20)/53 9b OTHER REPORT NO(S) (Any other numbers that may be assigned this report)

10 AVAILABILITY/LIMITATION NOTICES

Qualified Requesters may obtain copies of this report from DDC

11 SUPPLEMENTARY NOTES	12 SPONSORING MILITARY ACTIVITY
	Office of Naval Research Boston Branch Office, 495 Summer Street Boston 10, Massachusetts

13 ABSTRACT

Several specimens of commercial and high-purity lead of various grain size and crystallographic orientation were loaded dynamically in compression by means of the split Hopkinson bar. Strain rate was held constant at approximately 1200 sec^{-1} for strains up to about 15%. The dynamic stress-strain curves were found to lie approximately 50% higher than the corresponding static curves.

The compression tests described formed part of a larger project whose purpose was to determine dynamic values of Tabor's constant for lead and its dependence on crystal orientation. For this purpose the results of the compression tests were combined with those of dynamic indentation tests previously performed on the same lead specimens. It was found that dynamic values of Tabor's constant range from 2.4 to 6.0 depending upon grain size and orientation. These values are approximately equal to the corresponding static values. They may be compared to the value of 2.8 obtained by Tabor and other investigators for numerous fine-grained polycrystalline materials, including lead, and for strains up to about 20%.

DD FORM 1 JAN 64 1473

Security Classification

Security Classification

14. KEY WORDS	LINK A		LINK B		LINK C	
	ROLE	WT	ROLE	WT	ROLE	WT
Stress-strain relation (dynamic)						
Grain structure						

INSTRUCTIONS

1. ORIGINATING ACTIVITY: Enter the name and address of the contractor, subcontractor, grantee, Department of Defense activity or other organization *(corporate author)* issuing the report.

2*a*. REPORT SECURITY CLASSIFICATION: Enter the overall security classification of the report. Indicate whether "Restricted Data" is included. Marking is to be in accordance with appropriate security regulations.

2*b*. GROUP: Automatic downgrading is specified in DoD Directive 5200.10 and Armed Forces Industrial Manual. Enter the group number. Also, when applicable, show that optional markings have been used for Group 3 and Group 4 as authorized.

3. REPORT TITLE: Enter the complete report title in all capital letters. Titles in all cases should be unclassified. If a meaningful title cannot be selected without classification, show title classification in all capitals in parenthesis immediately following the title.

4. DESCRIPTIVE NOTES: If appropriate, enter the type of report, e.g., interim, progress, summary, annual, or final. Give the inclusive dates when a specific reporting period is covered.

5. AUTHOR(S): Enter the name(s) of author(s) as shown on or in the report. Enter last name, first name, middle initial. If military, show rank and branch of service. The name of the principal author is an absolute minimum requirement.

6. REPORT DATE: Enter the date of the report as day, month, year; or month, year. If more than one date appears on the report, use date of publication.

7*a*. TOTAL NUMBER OF PAGES: The total page count should follow normal pagination procedures, i.e., enter the number of pages containing information.

7*b*. NUMBER OF REFERENCES: Enter the total number of references cited in the report.

8*a*. CONTRACT OR GRANT NUMBER. If appropriate, enter the applicable number of the contract or grant under which the report was written.

8*b*, 8*c*, & 8*d*. PROJECT NUMBER: Enter the appropriate military department identification, such as project number, subproject number, system numbers, task number, etc.

9*a*. ORIGINATOR'S REPORT NUMBER(S): Enter the official report number by which the document will be identified and controlled by the originating activity. This number must be unique to this report.

9*b*. OTHER REPORT NUMBER(S). If the report has been assigned any other report numbers *(either by the originator or by the sponsor)*, also enter this number(s).

10. AVAILABILITY/LIMITATION NOTICES: Enter any limitations on further dissemination of the report, other than those imposed by security classification, using standard statements such as:

(1) "Qualified requesters may obtain copies of this report from DDC."

(2) "Foreign announcement and dissemination of this report by DDC is not authorized."

(3) "U. S. Government agencies may obtain copies of this report directly from DDC. Other qualified DDC users shall request through _____."

(4) "U. S. military agencies may obtain copies of this report directly from DDC. Other qualified users shall request through _____."

(5) "All distribution of this report is controlled. Qualified DDC users shall request through _____."

If the report has been furnished to the Office of Technical Services, Department of Commerce, for sale to the public, indicate this fact and enter the price, if known.

11. SUPPLEMENTARY NOTES: Use for additional explanatory notes.

12. SPONSORING MILITARY ACTIVITY. Enter the name of the departmental project office or laboratory sponsoring *(paying for)* the research and development. Include address.

13. ABSTRACT: Enter an abstract giving a brief and factual summary of the document indicative of the report, even though it may also appear elsewhere in the body of the technical report. If additional space is required, a continuation sheet shall be attached.

It is highly desirable that the abstract of classified reports be unclassified. Each paragraph of the abstract shall end with an indication of the military security classification of the information in the paragraph, represented as *(TS)*, *(S)*, *(C)*, or *(U)*.

There is no limitation on the length of the abstract. However, the suggested length is from 150 to 225 words.

14 KEY WORDS. Key words are technically meaningful terms or short phrases that characterize a report and may be used as index entries for cataloging the report. Key words must be selected so that no security classification is required. Identifiers, such as equipment model designation, trade name, military project code name, geographic location, may be used as key words but will be followed by an indication of technical context. The assignment of links, rules, and weights is optional.